Chemically Directed Assembly of Photoactive Metal Oxide Nanoparticle Heterojunctions *via* the Copper-Catalyzed Azide–Alkyne Cycloaddition "Click" Reaction

Allison C. Cardiel, Michelle C. Benson, Lee M. Bishop, Kacie M. Louis, Joseph C. Yeager, Yizheng Tan, and Robert J. Hamers*

Department of Chemistry, University of Wisconsin–Madison, 1101 University Avenue, Madison, Wisconsin 53706, United States

ABSTRACT

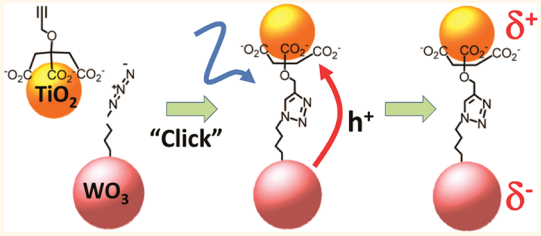

Metal oxides play a key role in many emerging applications in renewable energy, such as dye-sensitized solar cells and photocatalysts. Because the separation of charge can often be facilitated at junctions between different materials, there is great interest in the formation of heterojunctions between metal oxides. Here, we demonstrate use of the copper-catalyzed azide–alkyne cycloaddition reaction, widely referred to as "click" chemistry, to chemically assemble photoactive heterojunctions between metal oxide nanoparticles, using WO_3 and TiO_2 as a model system. X-ray photoelectron spectroscopy and Fourier-transform infrared spectroscopy verify the nature and selectivity of the chemical linkages, while scanning electron microscopy reveals that the TiO_2 nanoparticles form a high-density, conformal coating on the larger WO_3 nanoparticles. Time-resolved surface photoresponse measurements show that the resulting dyadic structures support photoactivated charge transfer, while measurements of the photocatalytic degradation of methylene blue show that chemical grafting of TiO_2 nanoparticles to WO_3 increases the photocatalytic activity compared with the bare WO_3 film.

KEYWORDS: metal oxide · click chemistry · photocatalysis · surface functionalization · dyads

The assembly of individual nanostructures into more complex structures can lead to novel properties of importance in fields such as renewable energy.[1–3] Metal oxide nanoparticles and nanostructured films are widely known for their photocatalytic properties, enabling conversion of sunlight into chemical energy.[4–8] The photocatalytic activity of such structures can often be enhanced through the use of heterojunctions between different oxides because the band offsets between the oxides can facilitate the separation of charge.[1,2] The WO_3/TiO_2 system[9–16] is particularly interesting because the valence and conduction bands of WO_3 both lie deeper in energy than those of TiO_2; this arrangement is often referred to as a "type II" band alignment and is particularly favorable for separation of photoexcited electrons and holes because the holes are energetically more stable in TiO_2 while the electrons are more stable in the WO_3. In addition, the 2.8 eV band gap of WO_3[17,18] (corresponding to a wavelength of ~440 nm) is smaller than that of anatase (3.2 eV), so that WO_3 enhances the ability of visible-light photons to induce photocatalytic activity. Photoexcitation of WO_3/TiO_2 heterojunctions at wavelengths shorter than ~440 nm leads to creation of electron–hole pairs in WO_3, followed by transfer of holes from WO_3 to TiO_2. Thus, the WO_3/TiO_2 heterojunction structure enhances the photooxidation activity by facilitating charge separation and by enabling excitation using light at longer wavelengths.[5,9,12,15]

The performance of WO_3/TiO_2 and other oxide/oxide heterojunctions is critically dependent on the ability to achieve intimate mixing and electrical contact between different materials.[14] Heterojunctions can be formed *via* a range of physical methods such as physical mixing[13,15] and sequential deposition methods.[14,19] The use of *chemical* assembly methods instead of the

* Address correspondence to rjhamers@wisc.edu.

Received for review September 18, 2011 and accepted December 24, 2011.

Published online December 24, 2011
10.1021/nn203585r

more commonly used physical methods provides an alternative, highly scalable approach to formation of heterojunctions between materials, especially when in nanoparticle form.[2,20] The Cu(I)-catalyzed azide–alkyne cycloaddition (CuAAC) reaction (often referred to as "click" chemistry)[21] has recently emerged as a particularly versatile way to achieve chemical assembly. While originally envisioned as a way to make molecule–molecule linkages, the CuAAC reaction has also been used to covalently bond molecules to extended surfaces[22–26] and to nanoparticles.[24,25,27–29] This reaction is of especially great interest because the triazole linkage formed upon reaction of an azide with an alkyne is a conjugated structure that supports electron transfer.[22,30,31]

Despite the widespread use of the CuAAC reaction to link small molecules to various substrates, the extension to the assembly of larger structures such as nanoparticle–surface or nanoparticle–nanoparticle junctions is much less explored.[32–34] Furthermore, while the ability to use the CuAAC reaction to form heterojunctions between semiconducting nanoparticles (such as between different metal oxides) could have great potential for applications such as novel photocatalysts and solar conversion, very few studies have explored the photoelectrochemical properties of CuAAC adducts.[23] Here, we demonstrate that the CuAAC reaction can be used to form photoelectrochemically active oxide/oxide nanoparticle heterojunctions, using the assembly of TiO_2 nanoparticles onto WO_3 nanoparticle thin films as a model system. Scanning electron microscopy (SEM) shows that the CuAAC reaction leads to highly conformal bonding of TiO_2 nanoparticles onto the WO_3 nanoparticle film. X-ray photoelectron spectroscopy (XPS) and Fourier-transform infrared (FTIR) spectroscopy measurements demonstrate that reaction occurs selectively between alkyne-functionalized TiO_2 and azide-functionalized WO_3 nanoparticles, while time-resolved surface photoresponse (TR-SPR) measurements directly reveal that TiO_2 nanoparticles enhance interfacial charge transfer. Finally, we demonstrate that the resulting WO_3/TiO_2 dyadic structures enhance the photo-oxidative breakdown of methylene blue, as a model photocatalytic reaction. These results show that the use of the CuAAC reaction provides a pathway toward formation of photoactive nanoparticle heterojunctions of relevance to emerging applications in renewable energy.

RESULTS

Formation of WO_3/TiO_2 Nanoparticle Heterojunctions *via* CuAAC Reaction. To make WO_3/TiO_2 nanoparticle heterojunctions, we first made a thin film of WO_3 nanoparticles and modified the WO_3 nanoparticles with azide groups by photochemically grafting 3-buten-1-ol to the nanoparticles and then converting the exposed

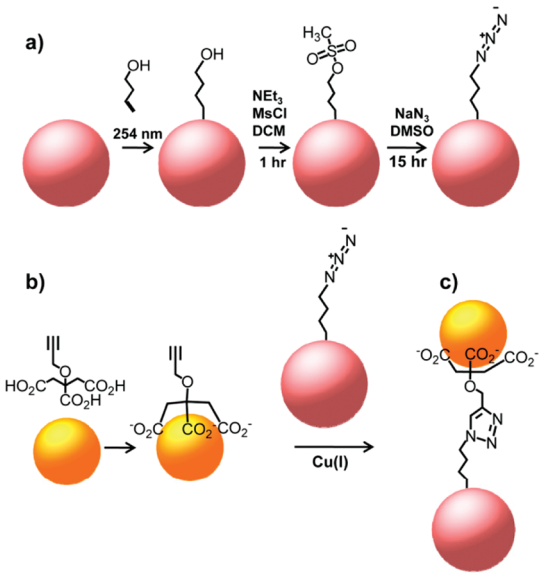

Figure 1. Schematic illustration showing steps in functionalization. (a) Azide functionalization of WO_3 nanoparticles, (b) functionalization of TiO_2 nanoparticles with *O*-propargyl citrate, and (c) CuAAC reaction to form WO_3/TiO_2 nanoparticle heterojunction.

–OH groups to azide groups using an intermediate mesylation step, as depicted in Figure 1a. The TiO_2 nanoparticles were synthesized and modified with alkyne group *via* adsorption of *O*-propargyl citrate, as shown in Figure 1b.[29] This ligand provides enhanced water stability compared with alternative monodentate ligands.[29] The conditions for the CuAAC reaction on WO_3 were optimized using the molecule 4-(trifluoromethoxy) phenyl acetylene (TFMPA), as described in the Materials and Methods section. These optimized conditions were then used to link the alkyne-modified TiO_2 nanoparticles to the WO_3 nanoparticle films *via* the CuAAC reaction to form the chemically assembled WO_3/TiO_2 adducts depicted in Figure 1c. Detailed procedures for each step depicted in Figure 1 are described in the Materials and Methods section.

SEM Imaging of Chemically Assembled Nanoparticle Heterojunctions. To confirm successful chemical assembly of TiO_2 nanoparticles onto the WO_3 nanoparticle film, we used scanning electron microscopy to visualize the WO_3 films before and after reaction. Figure 2 shows SEM images of the bare WO_3 surface and a WO_3 surface after the CuAAC reaction with the TiO_2 nanoparticles. The bare WO_3 film shows nanoparticles ~50 nm in diameter, with no surface features visible on the particles. After functionalization with the TiO_2 nanoparticles, the SEM images clearly show TiO_2 nanoparticles conformally coating the WO_3 nanoparticles. A cross-section of the full WO_3 film after grafting of TiO_2 nanoparticles established that the TiO_2 nanoparticles were able to penetrate and functionalize ~100 nm deep into a ~200 nm thick WO_3 nanocrystalline film.

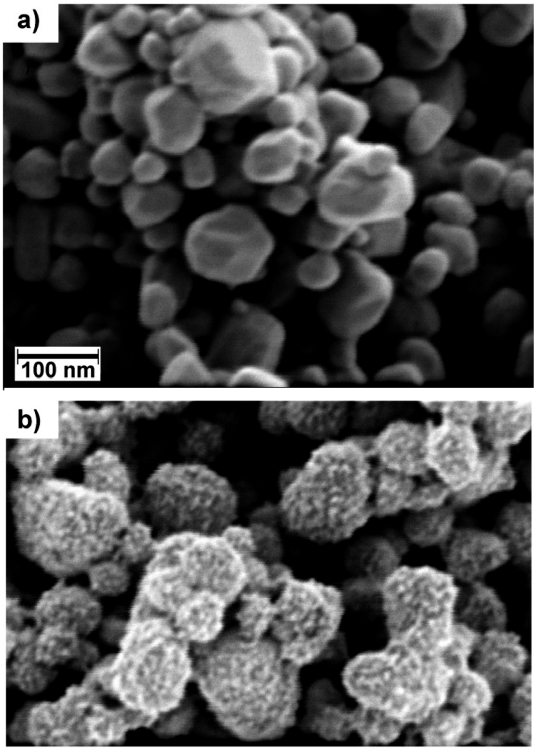

Figure 2. Bare nanocrystalline WO_3 film before and after CuAAC reaction with alkyne-modified TiO_2 nanoparticles: (a) before reaction, (b) after reaction to form the WO_3/TiO_2 adduct.

Chemical Characterization of CuAAC Linking Chemistry. We used X-ray photoelectron spectroscopy and Fourier-transform infrared spectroscopy to characterize the CuAAC reaction and included control experiments to establish that the formation of the WO_3/TiO_2 nanoparticle adducts occurred selectively as a consequence of the CuAAC chemistry and not from nonspecific interactions such as electrostatic or dispersion forces.[35] Figure 3 shows XPS data from WO_3 nanoparticle films that were carried through the full reaction sequence ("full CuAAC") to yield the nanoparticle−nanoparticle adduct depicted in Figure 1c, along with data obtained from two control samples. The "no azide" control consists of a WO_3 nanoparticle film that was modified with butenol and carried through the entire reaction sequence, except the mesylation and azidation steps (see Figure 1a) were eliminated; assuming perfectly selective coupling between the azide and alkyne groups with no other side reactions, this sample should therefore correspond to a butenol-modified WO_3 surface. The "no Cu" control sample consists of a WO_3 sample that was carried through the entire reaction sequence, except that the Cu/TBTA solution was replaced with neat DMSO for the final coupling step of Figure 1b; assuming perfectly selective chemistry, this sample should correspond to an azide-modified WO_3 surface.

In Figure 3, the N(1s) peak near 404.5 eV for the "no Cu" control is characteristic of the positively charged

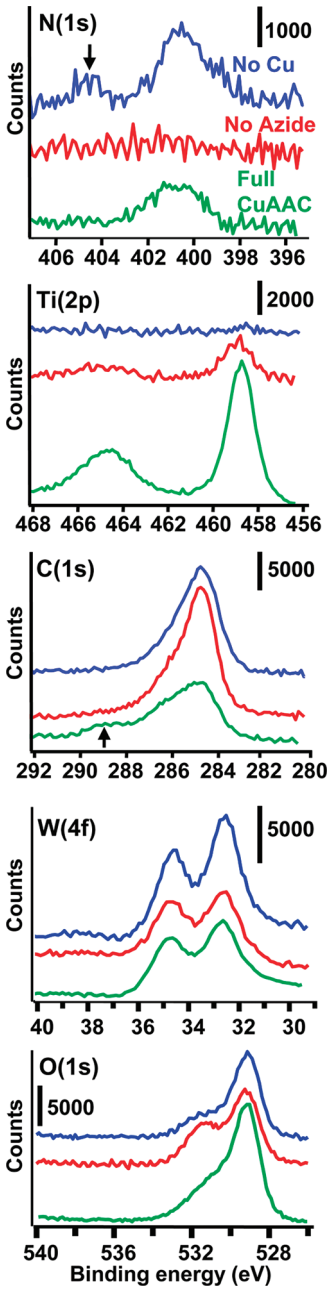

Figure 3. XPS data for azide-modified WO_3 sample exposed to alkyne-modified TiO_2 nanoparticles, including full CuAAC reaction conditions (bottom line, green) and no Cu (middle line, blue) and no azide (bottom line, red) control samples as described in the text.

N atom of the $-N{=}N^{+}{=}N^{-}$ azide resonance structure. The presence of this peak on the "no Cu" control verifies successful functionalization of the WO_3 nanoparticle film with azide groups; the *absence* of this peak on the "full CuAAC" sample is consistent with reaction of the azide groups to form the interfacial triazole ring (see Figure 1c), which yields N(1s) peaks near 400.0 and 401.5 eV. The Ti(2p) data for the "no azide" control and the "no Cu" control sample show only minimal intensity, while the "full CuAAC" sample shows a much larger signal; thus, the Ti(2p) data show that grafting of

alkyne-modified TiO_2 nanoparticles to the WO_3 nanoparticle film is selective, requiring the presence of both the azide groups and the Cu(I) catalyst. The C(1s) data (Figure 3c) are difficult to analyze because small amounts of carbon contamination are unavoidable in benchtop chemistry; however, the "full CuAAC" sample shows a C(1s) feature at a high binding energy of 289 eV (indicted by an arrow) not present on the other samples; this high binding energy is characteristic of C═O moieties within carboxylate groups and is similar to that observed from acetic anhydride adsorbed on TiO_2.[36] The presence of this peak confirms that the TiO_2 nanoparticles grafted onto the WO_3 surface remain functionalized with the *O*-propargyl citrate ligand (Figure 1b), which has three carboxylate groups per molecule. The W(4f) and O(1s) data show little change during the reaction sequence, except that the W(4f) signal becomes slightly attenuated while the O(1s) signal is slightly enhanced after reaction; these changes are consistent with linking TiO_2 nanoparticles onto the WO_3 film.

Figure S6 and S7 in the Supporting Information show XPS survey spectra after formation of the WO_3/TiO_2 adduct, a "no azide" control sample of a butenol-modified WO_3 film (without subsequent mesylation or azidation steps) that was exposed to the alkyne-modified TiO_2 with the Cu catalyst, and a WO_3 sample functionalized *via* the CuAAC reaction with TFMPA. Figure S6 shows no detectable contamination except for small amounts of Na. In particular, Figure S7 shows an expanded view of the 920−950 eV region where the primary Cu(2p) peaks are; even on this expanded scale there is no detectable intensity from Cu. Thus, while Cu is used as a catalyst in the CuAAC reaction, there is no detectable copper remaining on any of the functionalized surfaces. Our data indicate that the organic layers used in the reactions effectively prevent Cu ions from binding to the nanoparticle surfaces.

Figure 4 shows FTIR data at different stages of the CuAAC reaction sequence. The butenol-modified surface is dominated by the $-CH_2$ features near 2900 cm^{-1}. The azide-modified surface shows a pronounced peak at 2098 cm^{-1} due to the azide group. After reaction, this azide peak is reduced in intensity. We note that because of geometric constraints not all azide groups are expected to be able to bind to the roughly spherical TiO_2 nanoparticles, and therefore the persistence of some azide group after reaction is consistent with expectations. The nanoparticle solution also likely contains some excess *O*-propargylcitric acid that is not completely removed by dialysis; these ligands can also react with azide groups that are not accessible to the TiO_2 nanoparticle due to the above-mentioned packing constraints.

Photoelectrochemical Response. To determine how the chemical assembly of TiO_2 nanoparticles onto the WO_3 nanoparticle film altered the photoelectrochemical response, we used time-resolved surface photoresponse measurements to characterize the photoinduced charge transfer. While most studies of photoelectrochemical response measure the long-time behavior that is largely dominated by diffusion and recombination in the bulk,[37,38] our studies focused on investigating the faster (nanosecond-scale) charge-transfer processes characteristic of the surface region. In these measurements a short laser pulse (here, ~3 ns duration) was used to illuminate the sample, creating photoexcited electron−hole pairs. Separation of these electron−hole pairs at the interface created a transient capacitive displacement current that was measured and recorded using a fast digital oscilloscope. The measured transient displacement current can be presented directly or can be integrated to show the time-dependent transfer of charge, Q_{trans}. The maximum value of Q_{trans} is a measure of the extent of charge transfer induced at the surface by each pulse of light. Figure 5b shows the Q_{trans} *vs* time measured at one wavelength, here arbitrarily chosen to be 550 nm. Figure 5c shows the magnitude of Q_{trans} as a function of excitation wavelength for a WO_3/TiO_2 adduct structure like that shown in Figure 2, along with a bare WO_3 nanocrystalline film, a film after grafting with butenol, and a WO_3 sample that was functionalized with butenol and carried through all steps to undergo the CuAAC reaction with TFMPA. In each case Q_{trans} was normalized to a constant fluence of 700 μJ/pulse to account for slight variations in laser fluence with wavelength. Figure 5d shows the external absorbance (*i.e.*, absorbance uncorrected for reflection losses) of the same film. It shows a broad onset to absorption near 450 nm, although it is difficult to separate absorption from scattering and reflection losses in nanocrystalline films. The spectrum is consistent within previous studies showing that WO_3 nanocrystalline films have a broad absorption edge near ~440 nm with a tail extending out past 470 nm.[39] In contrast, TiO_2 does not absorb appreciably at wavelengths > 400 nm.

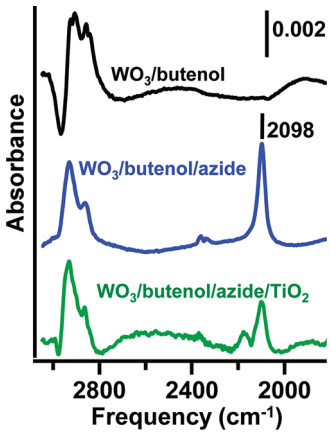

Figure 4. FTIR spectra of WO_3 nanoparticle films at different stages of functionalization.

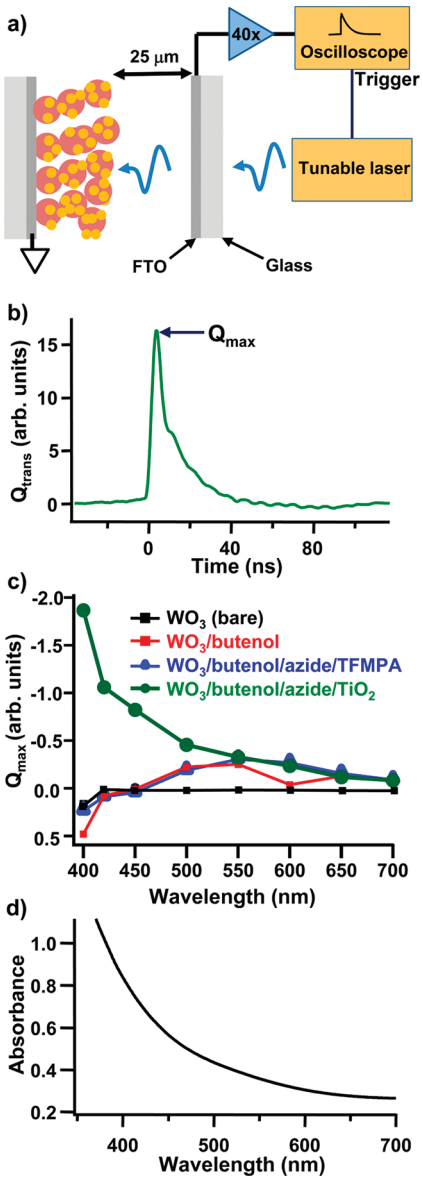

Figure 5. (a) Time-resolved surface photoresponse measurement. (b) Time-dependent charge transfer from WO_3/TiO_2 adduct. (c) Wavelength dependence of maximum charge transfer Q_{max} for TiO_2 nanoparticles linked to WO_3 and for control samples described in the text. (d) Absorption spectrum of WO_3 film, not corrected for scattering or reflection losses.

The data in Figure 5c show that the wavelength dependence of the photoelectric response from the WO_3/TiO_2 adduct is similar to that of the measured absorbance (Figure 5d). At wavelengths between ~400 and ~450 nm, where bulk WO_3 absorbs but TiO_2 does not, the photovoltaic response from the covalently bonded WO_3/TiO_2 dyadic structures is large, with the sign of the charge transfer corresponding to accumulation of holes at the outermost surface (*i.e.*, the TiO_2 nanoparticle layer). This is the expected behavior if the absorption of light in WO_3 or TiO_2 creates electron pairs with the holes preferentially trapped on the TiO_2 nanoparticles. The bare WO_3 surface shows no significant response throughout the entire visible region. A small positive response is also observed in the midvisible (~500−600 nm) range from all the samples that have been functionalized *via* the photochemical grafting procedure. At the very shortest wavelength all samples that have been functionalized with molecular layers *via* the UV grafting method show a change in sign corresponding to accumulation of negative charge at the surface. WO_3 is widely known for its photochromic behavior when illuminated with UV light,[13] and our results suggest that the UV grafting process may affect the trapping of charges within WO_3. The data in Figure 5c clearly demonstrate that the coupling of TiO_2 nanoparticles to the WO_3 nanocrystalline film *via* the CuAAC reaction significantly enhances the accumulation of positive charges at the outermost surface when illuminated with visible light in the 400−500 nm region.

Photocatalytic Activity. To test whether the assembly of TiO_2 nanoparticles onto the WO_3 nanoparticle film altered the photocatalytic activity, we investigated the photochemical degradation of methylene blue (MB) solutions in contact with the nanoparticle films. Samples of interest were immersed into spectrophotometer cuvettes containing a solution of methylene blue (4.0 μM in water); the samples were then illuminated with monochromatic light at a wavelength of 365 nm. After specific times the UV−visible absorption spectrum of each solution was measured. Figure 6a shows absorption spectra from the MB solution in contact with the WO_3/TiO_2 adducts. MB gives rise to a large absorption peak at 663 nm. As the illumination time is increased, this peak is reduced in intensity. At the longest times, the absorption peak also appears to shift slightly to shorter wavelength, likely due to a small amount of absorbance from the decomposition products.

Figure 6b shows the absorbance at 663 nm (at or near the peak absorbance) *vs* time for several different samples, along with fits of the absorbance $A(t)$ to a first-order decay, $A(t) = A_0 \exp^{-kt}$, where k is the rate constant and A_0 is the absorbance at time $t = 0$.[15] The individual measurements were normalized to the measured absorbance at $t = 0$ to account for slight variations in MB concentration in different experiments. The sample made by chemical assembly of TiO_2 nanoparticles onto the WO_3 surface yielded a rate constant of $k = (2.7 \pm 0.1) \times 10^{-3}$ min^{-1}, while the bare WO_3 surface yielded $(1.40 \pm 0.07) \times 10^{-3}$ min^{-1}. A pure methylene blue solution (with no immersed sample) yielded an immeasurably low value of $k < 1 \times 10^{-5}$ min^{-1}, statistically indistinguishable from zero. Similarly, control experiments using an uncoated Si substrate showed no detectable degradation of methylene blue. These experiments show that chemical assembly of TiO_2 nanoparticles onto the WO_3 nanocrystalline film increases the photocatalytic efficiency by approximately

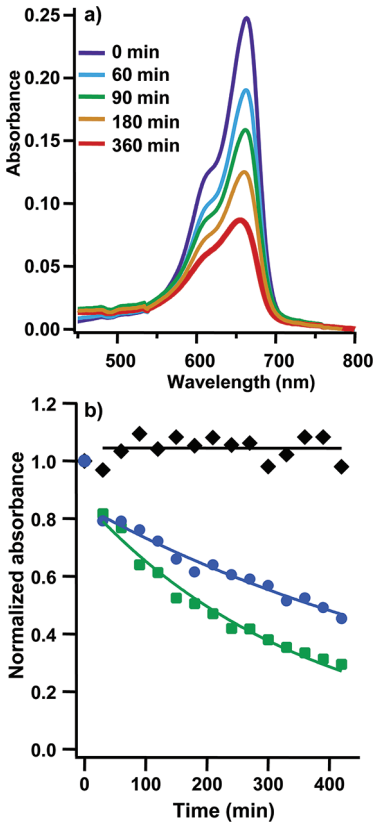

Figure 6. (a) UV−visible absorption spectrum of methylene blue in contact with the WO_3/TiO_2 adduct after indicated illumination times. (b) Absorbance at 663 nm *vs* time for methylene blue solution (black) and for MB solution in contact with UV-illuminated samples of WO_3 (blue) and WO_3/TiO_2 adduct (green). Solid lines are fits to exponential decays.

a factor of 2. While many factors such as the presence of surface states can affect the overall photocatalytic activity, these results show that the chemically assembled WO_3/TiO_2 heterojunction structures are photocatalytically active.

DISCUSSION

The results presented above show two important facts: first, that the CuAAC reaction can be used to create heterojunctions between different metal oxide nanoparticles using selective reactions that form robust chemical linkages; second, that the resulting nanoparticle heterojunctions are photoelectrochemically active, able to support charge transfer that enhances photocatalytic activity. These results suggest the possibility of using the CuAAC reaction as a pathway toward formation of a wider variety of charge-separating heterojunction structures. Heterojunctions between different semiconductors are important because the offset of valence and conduction bands can enhance the separation of charge, thereby reducing recombination rates and enhancing photocatalytic activity.[40−45] TiO_2 has a band gap of 3.2 eV (corresponding to a wavelength ~385 nm), but because it is an indirect gap semiconductor, the

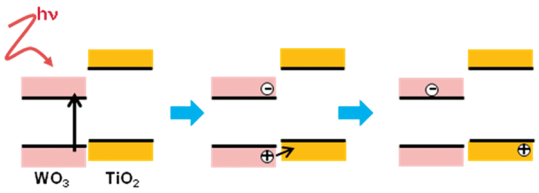

Figure 7. Successive stages in photoinitiated charge transfer at WO_3/TiO_2 junction, including absorption (left), hole migration (center), and resulting separated electron−hole pair (right).

absorption is weak at wavelengths longer than ~350 nm.[46] WO_3 has a band gap of ~2.8 eV[17,18] and so absorbs light at wavelengths shorter than ~440 nm. More importantly, previous studies have shown that valence and conduction bands of WO_3 are both lower in energy than those of TiO_2, leading to a staggered "type II" band alignment depicted in Figure 7a.[11,47] A consequence of this alignment is that when electron−hole pairs are created by absorption of light in WO_3 (Figure 7a), the valence-band holes are expected to preferentially migrate to the TiO_2 (Figure 7b) while the conduction-band electrons are expected to remain in the WO_3. Thus, the WO_3/TiO_2 heterojunction induces charge separation that facilitates electrochemical oxidation reactions at the TiO_2 surface and reduction reactions at WO_3 (Figure 7c).[11,12,47]

Our results show that the CuAAC reaction plays a critical role in the assembly of the nanoparticle structures. It is less clear whether subsequent charge-transfer processes occur through the molecular assembly or whether the nanoparticles achieve direct nanoparticle−nanoparticle contact. While our results show that the binding of the TiO_2 nanoparticles to the WO_3 nanoparticle film is clearly controlled by the formation of chemical bonds during the CuAAC reaction, subsequent rinsing and drying steps also introduce capillary forces between the TiO_2 nanoparticles and the underlying WO_3 film. The capillary force between a nanoparticle and an underlying substrate can be roughly estimated as $F = 4\pi R\sigma \cos(\theta)$, where R is the particle radius, σ is the interfacial tension, and θ is the contact angle.[48] Using $R = 3$ nm, $\sigma = 7.0 \times 10^{-3}$ N/m, and $\theta = 75°$ (a value typical of TiO_2 with organic layers)[49] yields a force of 2×10^{-9} Newton. Estimating this is distributed over a radius of 1 nm yields a pressure of 2×10^8 N/m^2, or 0.2 GPa. Pressures of this magnitude are in the range where a transition from fluid-like to solid-like behavior has been observed in studies of self-assembled monolayers using atomic force microscopy.[50] While further studies will be necessary to develop a more detailed understanding of how the molecules impact transfer processes, our results show that the CuAAC reaction using short molecular ligands can be used to assemble oxide/oxide nanoparticle heterojunctions that enhance charge transfer and photocatalytic activity.

CONCLUSIONS

Our results show that the CuAAC "click" reaction can be used to chemically assemble heterojunctions between metal oxide nanoparticles and that when illuminated the resulting WO_3/TiO_2 adducts support charge transfer and exhibit enhanced photocatalytic activity compared with the WO_3 surface alone. These results suggest that the use of "click" chemistry may enable a broad range of applications in the chemical assembly of novel charge-transporting heterostructures.

MATERIALS AND METHODS

WO_3 Nanoparticle Thin Film Preparation. The WO_3 nanoparticle paste was created following a slight variation of previously published procedures[51,52] by adding 10 g of a 10% solution of Butvar (Aldrich) in absolute ethanol to 2 g of WO_3 nanopowder (30−70 nm diameter, Nanostructured & Amorphous Materials), followed by 8 g of terpineol (Aldrich) and an additional 10 mL of absolute ethanol. The mixture was ultrasonically agitated for 90 min, and the excess solvent was removed using rotary evaporation, forming a paste. The paste was screen-printed onto a substrate, giving a circular film 5 mm in diameter. Most experiments used substrates of fluorinated tin oxide on glass (sheet resistance 15 Ω/sq, Hartford Glass) that served as a conductive and transparent substrate. Some scanning electron microscopy experiments were performed using thin films screen-printed onto heavily doped silicon wafers; because Si substrates are flatter than FTO, Si substrates give better measurement of the nanoparticle film thickness. Methylene blue photodegradation experiments were carried out using thin films screen-printed onto Si substrates. Following screen-printing the films were sintered at 140 °C for 20 min followed by additional heating at 500 °C for 1 h. The resulting films were approximately 200 nm thick, consisting of particles that were 30−70 nm in diameter. A Raman spectrum of the resulting film is presented in the Supporting Information (Figure S1). The frequencies and intensities of the peaks are in close agreement with those reported previously for the monoclinic $P2_1/m$ (γ-WO_3) phase.[53]

WO_3 Nanoparticle Thin Film Functionalization. WO_3 nanoparticle thin films were functionalized with a terminal azide group using a procedure similar to that reported for SnO_2 thin films.[23] This procedure is depicted in Figure 1a. The WO_3 nanoparticle film was covered with a thin layer of 3-buten-1-ol and then sealed in an Ar-purged cell in an Ar glovebox. The cell was then exposed to ultraviolet (UV) light (254 nm, ∼15 mW/cm^2) for 15 h to graft the 3-buten-1-ol molecules to the WO_3 surface *via* the alkene group. The samples were then rinsed sequentially with methanol (MeOH), $CHCl_3$, and isopropyl alcohol (IPA). The terminal −OH groups were converted to methanesulfonyl (mesyl) groups by immersing the sample in a 10:1:1 (by volume) dichloromethane (DCM)/triethylamine (NEt_3)/methanesulfonyl chloride (MsCl) mixture for 1 h in an ice bath. After rinsing with DCM, MeOH, and IPA for 30 s each the mesyl groups were converted to azide groups by immersing the sample in a solution of supersaturated NaN_3 in dimethylsulfoxide (DMSO) for 15 h at 80 °C. Rinsing with deionized water for one minute followed by IPA for 30 s resulted in azide-modified surfaces.

Preparation of Alkyne-Modified TiO_2 Nanoparticles. Bare TiO_2 nanoparticles were synthesized using procedures described by Kotsokechagia *et al.*,[54] as detailed in the Supporting Information. The size distribution of the TiO_2 nanoparticles was characterized by transmission electron microscopy (TEM). Figure S2 of the Supporting Information shows a representative TEM image of the TiO_2 nanoparticles dispersed on lacey carbon. Size analysis yielded an average diameter of 5.9 nm, with a standard deviation of 1.1 nm.

The TiO_2 nanoparticles were functionalized with alkyne groups using *O*-propargylcitric acid, a citric acid derivative bearing an alkyne group, as described previously.[29] Functionalization was accomplished by first precipitating the nanoparticles from the acidic storage solution by addition of a mixture of 3:1 (v:v) diethyl ether/MeOH. The cloudy precipitate was agitated to completely homogenize the contents; the mixture was then centrifuged (5000 rpm for 10 min), and the supernatant was then decanted. *O*-Propargylcitric acid (10 mM in MeOH) was added to the nanoparticle precipitate, and the resulting mixture was agitated to resuspend the nanoparticles. The suspension was ultrasonically agitated for 1.5 h to yield a translucent suspension, which was then dialyzed using a cellulose membrane (Sigma Aldrich #D9777, molecular weight cutoff 12 400 Da) in MeOH for 48 h. The dialysis solution was refreshed after 24 h. The samples were stored in the dark until use. Successful functionalization was assessed using transmission-mode FTIR spectroscopy by placing a small amount of the suspension onto a salt plate and evaporating the MeOH at 80 °C. The appearance of absorbance bands that are characteristic of *O*-propargyl citrate bound onto the TiO_2 nanoparticles was observed at 1380−1460 and 1540−1620 cm^{-1}; these spectra are shown in the Supporting Information, Figure S3.

CuAAC Reaction between Azide-Modified WO_3 Nanoparticle Film and Alkyne-Modified TiO_2 Nanoparticles. Optimum conditions for the CuAAC reaction were identified by reacting the WO_3 nanoparticle films with 4-(trifluoromethoxy)phenylacetylene (TFMPA). In addition to having an alkyne group, this molecule has F atoms that serve as good markers in XPS. XPS data demonstrating the chemically selective reaction of TFMPA with the azide-modified WO_3 nanoparticles are shown in the Supporting Information. The optimized conditions were then used to make the WO_3/TiO_2 adducts. The azide-modified WO_3 nanoparticle film was immersed in a solution made from 0.5 mL of the of alkyne-modified TiO_2 nanoparticle suspension (2×10^{-4} M Ti concentration), 0.01 g of sodium ascorbate, 0.5 mL of water, and 1 mL of 2 mM copper/Tris[(1-benzyl-1*H*-1,2,3-triazol-4-yl)methyl]amine (Cu/TBTA) solution in DMSO for approximately 14 h. The samples were then sequentially rinsed with deionized water, MeOH, and IPA and then stored in IPA until use. To test whether the reactions occurred selectively between the azide- and alkyne-modified nanoparticles, control experiments were performed in which the mesylation and azidation steps were eliminated and by leaving out the Cu catalyst in the final coupling step.

Fourier-Transform Infrared (FTIR) Measurements. Infrared spectra were collected using an FTIR spectrometer (Vertex 70, Bruker Optics, Billerica, MA, USA) at a resolution of 4 cm^{-1} in single-bounce external reflection mode using a variable-angle specular reflectance accessory with a wire grid polarizer (VeeMAX II, Pike Technologies, Madison, WI, USA). All reflection spectra were collected with p-polarized light at an incident angle of 50° from the surface normal. FTIR spectra of functionalized surfaces were measured using an unfunctionalized sample as the background. Residual baselines were removed to improve the clarity of the spectra. Baseline correction was achieved using a polynomial fit to remove sloping and/or curved background. In this procedure a single polynomial was fit to each spectrum, including only regions where no absorption features were present.

X-ray Photoelectron Spectroscopy Measurements. XPS data were obtained using a custom-built XPS system (Physical Electronics Inc., Eden Prairie, MN, USA) consisting of a model 10-610 Al Kα source (1486.6 eV photon energy) with a model 10-420 toroidal monochromator and a model 10-360 hemispherical analyzer with a 16-channel detector array; measurements were typically performed using a electron takeoff angle of 45° and an analyzer pass energy of 58.75 eV (yielding an analyzer resolution of 0.88 eV). Peak areas were calculated by fitting the raw data to Voigt functions after a Shirley baseline correction.[55] The spectra of each sample were shifted as necessary to make the primary C(1s) peak lie at a fixed energy of 284.8 eV;[56] all other spectra for a given sample were shifted by the same amount.

Time-Resolved Surface Photoresponse Measurements. Time-resolved surface photoresponse measurements[57−59] were performed using a custom-made cell holder in which a sense electrode was held 25 μm away from the sample surface. The entire cell was sealed inside an argon glovebox. The sample was illuminated with short pulses (<3 ns, ~700 μJ/pulse) from a tunable laser system (NT340, Ekspla, Inc., Vilnius, Lithuania); the resulting separation of charges induced a transient change in surface potential that was sensed *via* the displacement current induced in the adjacent sense electrode, which was connected directly to the input of a fast amplifier (model TA2000B-3, FAST ComTec GmbH, Oberhaching/München, Germany) with 50 Ω input and output impedances, 1.5 GHz bandwidth, and 40× voltage gain. The amplified output was recorded on a sampling digital oscilloscope (model DSO5054A, Agilent, Inc., Santa Clara, CA, USA).

Photochemical Activity Measurements. Photochemical activity measurements were performed by immersing the sample (5 mm diameter active region) in a cuvette containing a 4×10^{-6} M solution of methylene blue in water and illuminating with 365 nm light from a long-wave ultraviolet lamp (Spectroline ENB-260C) with a flux of ~3.1 mW/cm^2 at the sample. At this wavelength the absorption by the TiO_2 nanoparticles is negligible.[57−59] The absorbance of the methylene blue was measured as a function of time using a Shimadzu UV−visible spectrophotometer, and the rate of decomposition was extracted from the change in absorbance *vs* time.

Acknowledgment. This work was supported by the U.S. Department of Energy Office of Basic Energy Sciences contract DE-FG02-09ER16122. A.C.C. was partially supported by Carleton College Summer Science Fellowship and the UW-Madison Research Experience for Undergraduates Program, NSF CHE-1004690.

Supporting Information Available: Raman spectrum of WO_3 nanoparticles, synthesis of TiO_2 nanoparticles, transmission electron microscopy of TiO_2 nanoparticles, infrared spectra of TiO_2 nanoparticles functionalized with *O*-propargyl citrate, and optimization of CuAAC reaction. XPS spectra of WO_3 at different stages of functionalization, after WO_3/TiO_2 adduct formation, and control samples. This material is available free of charge *via* the Internet at http://pubs.acs.org.

REFERENCES AND NOTES

1. Jin, R. C.; Wu, G. S.; Li, Z.; Mirkin, C. A.; Schatz, G. C. What Controls the Melting Properties of DNA-Linked Gold Nanoparticle Assemblies? *J. Am. Chem. Soc.* **2003**, *125*, 1643–1654.
2. Robel, I.; Subramanian, V.; Kuno, M.; Kamat, P. V. Quantum Dot Solar Cells. Harvesting Light Energy with Cdse Nanocrystals Molecularly Linked to Mesoscopic TiO_2 Films. *J. Am. Chem. Soc.* **2006**, *128*, 2385–2393.
3. Guo, Y. G.; Hu, Y. S.; Sigle, W.; Maier, J. Superior Electrode Performance of Nanostructured Mesoporous TiO_2 (Anatase) through Efficient Hierarchical Mixed Conducting Networks. *Adv. Mater.* **2007**, *19*, 2087–2091.
4. Fujishima, A.; Honda, K. Electrochemical Photolysis of Water at a Semiconductor Electrode. *Nature* **1972**, *238*, 37–38.
5. Fu, X. Z.; Clark, L. A.; Yang, Q.; Anderson, M. A. Enhanced Photocatalytic Performance of Titania-Based Binary Metal Oxides: TiO_2/SiO_2 and TiO_2/ZrO_2. *Environ. Sci. Technol.* **1996**, *30*, 647–653.
6. Kudo, A.; Miseki, Y. Heterogeneous Photocatalyst Materials for Water Splitting. *Chem. Soc. Rev.* **2009**, *38*, 253–278.
7. Zou, Z. G.; Ye, J. H.; Sayama, K.; Arakawa, H. Direct Splitting of Water under Visible Light Irradiation with an Oxide Semiconductor Photocatalyst. *Nature* **2001**, *414*, 625–627.
8. Asahi, R.; Morikawa, T.; Ohwaki, T.; Aoki, K.; Taga, Y. Visible-Light Photocatalysis in Nitrogen-Doped Titanium Oxides. *Science* **2001**, *293*, 269–271.
9. Do, Y. R.; Lee, W.; Dwight, K.; Wold, A. The Effect of WO_3 on the Photocatalytic Activity of TiO_2. *J. Solid State Chem.* **1994**, *108*, 198–201.
10. Vermaire, D. C.; Vanberge, P. C. The Preparation of WO_3/TiO_2 and WO_3/Al_2O_3 and Characterization by Temperature-Programmed Reduction. *J. Catal.* **1989**, *116*, 309–317.
11. Kwon, Y. T.; Song, K. Y.; Lee, W. I.; Choi, G. J.; Do, Y. R. Photocatalytic Behavior of WO_3-Loaded TiO_2 in an Oxidation Reaction. *J. Catal.* **2000**, *191*, 192–199.
12. Li, X. Z.; Li, F. B.; Yang, C. L.; Ge, W. K. Photocatalytic Activity of WO_x-TiO_2 under Visible Light Irradiation. *J. Photochem. Photobiol. A* **2001**, *141*, 209–217.
13. He, T.; Ma, Y.; Cao, Y.; Hu, X. L.; Liu, H. M.; Zhang, G. J.; Yang, W. S.; Yao, J. N. Photochromism of WO_3 Colloids Combined with TiO_2 Nanoparticles. *J. Phys. Chem. B* **2002**, *106*, 12670–12676.
14. Irie, H.; Mori, H.; Hashimoto, K. Interfacial Structure Dependence of Layered TiO_2/WO_3 Thin Films on the Photoinduced Hydrophilic Property. *Vacuum* **2004**, *74*, 625–629.
15. Miyauchi, M.; Nakajima, A. K.; Watanabe, T.; Hashimoto, K. Photoinduced Hydrophilic Conversion of TiO_2/WO_3 Layered Thin Films. *Chem. Mater.* **2002**, *14*, 4714–4720.
16. Enesca, A.; Andronic, L.; Duta, A.; Manolache, S. Optical Properties and Chemical Stability of WO_3 and TiO_2 Thin Films Photocatalysts. *Rom. J. Inf. Sci. Technol.* **2007**, *10*, 269–277.
17. Gonzalez-Borrero, P. P.; Sato, F.; Medina, A. N.; Baesso, M. L.; Bento, A. C.; Baldissera, G.; Persson, C.; Niklasson, G. A.; Granqvist, C. G.; da Silva, A. F. Optical Band-Gap Determination of Nanostructured WO_3 Film. *Appl. Phys. Lett.* **2010**, *96*, 061909.
18. Migas, D. B.; Shaposhnikov, V. L.; Rodin, V. N.; Borisenko, V. E.; Tungsten Oxides., I. Effects of Oxygen Vacancies and Doping on Electronic and Optical Properties of Different Phases of WO_3. *J. Appl. Phys.* **2010**, *108*, 093713.
19. Lu, J. L.; Kosuda, K. M.; Van Duyne, R. P.; Stair, P. C. Surface Acidity and Properties of TiO_2/SiO_2 Catalysts Prepared by Atomic Layer Deposition: UV-Visible Diffuse Reflectance, DRIFTS, and Visible Raman Spectroscopy Studies. *J. Phys. Chem. C* **2009**, *113*, 12412–12418.
20. Litschauer, M.; Puchberger, M.; Peterlik, H.; Neouze, M.-A. Anion Methathesis in Ionic Silica Nanoparticle Networks. *J. Mater. Chem.* **2010**, *20*, 1269–1276.
21. Kolb, H. C.; Finn, M. G.; Sharpless, K. B. Click Chemistry: Diverse Chemical Function from a Few Good Reactions. *Angew. Chem., Int. Ed.* **2001**, *40*, 2004–2021.
22. Collman, J. P.; Devaraj, N. K.; Chidsey, C. E. D. "Clicking" Functionality onto Electrode Surfaces. *Langmuir* **2004**, *20*, 1051–1053.
23. Benson, M. C.; Ruther, R. E.; Gerken, J. B.; Rigsby, M. L.; Bishop, L. M.; Tan, Y.; Stahl, S. S.; Hamers, R. J. Modular "Click" Chemistry for Electrochemically and Photoelectrochemically Active Molecular Interfaces to Tin Oxide Surfaces. *ACS Appl. Mater. Interfaces* **2011**, *3*, 3110–3119.
24. White, M. A.; Maliakal, A.; Turro, N. J.; Koberstein, J. "Click" Dielectrics: Use of 1,3-Dipolar Cycloadditions to Generate Diverse Core-Shell Nanoparticle Structures with Applications to Flexible Electronics. *Macromol. Rapid Commun.* **2008**, *29*, 1544–1548.
25. Tchoul, M. N.; Fillery, S. P.; Koerner, H.; Drummy, L. F.; Oyerokun, F. T.; Mirau, P. A.; Durstock, M. F.; Vaia, R. A. Assemblies of Titanium Dioxide-Polystyrene Hybrid Nanoparticles for Dielectric Applications. *Chem. Mater.* **2010**, *22*, 1749–1759.
26. Watson, M. A.; Lyskawa, J.; Zobrist, C.; Fournier, D.; Jimenez, M.; Traisnel, M.; Gengembre, L.; Woisel, P. A "Clickable" Titanium Surface Platform. *Langmuir* **2010**, *26*, 15920–15924.
27. Gole, A.; Murphy, C. J. Azide-Derivatized Gold Nanorods: Functional Materials for "Click" Chemistry. *Langmuir* **2008**, *24*, 266–272.
28. White, M. A.; Johnson, J. A.; Koberstein, J. T.; Turro, N. J. Toward the Syntheses of Universal Ligands for Metal Oxide Surfaces: Controlling Surface Functionality through Click Chemistry. *J. Am. Chem. Soc.* **2006**, *128*, 11356–11357.
29. Bishop, L. M.; Yeager, J. C.; Chen, X.; Wheeler, J. N.; Torelli, M. C.; Benson, M. C.; Burke, S. D.; Pedersen, J. A.; Hamers, R. J.,

A Citric Acid-Derived Ligand for Modular Functionalization of Metal Oxide Surfaces *via* "Click" Chemistry. *Langmuir* **2011**, manuscript accepted, DOI 10.1021/la204145t.
30. Devaraj, N. K.; Decreau, R. A.; Ebina, W.; Collman, J. P.; Chidsey, C. E. D. Rate of Interfacial Electron Transfer through the 1,2,3-Triazole Linkage. *J. Phys. Chem. B* **2006**, *110*, 15955–15962.
31. Devadoss, A.; Chidsey, C. E. D. Azide-Modified Graphitic Surfaces for Covalent Attachment of Alkyne-Terminated Molecules by "Click" Chemistry. *J. Am. Chem. Soc.* **2007**, *129*, 5370–5371.
32. Kinge, S.; Gang, T. A.; Naber, W. J. M.; van der Wiel, W. G.; Reinhoudt, D. N. Magnetic Nanoparticle Assembly on Surfaces Using Click Chemistry. *Langmuir* **2011**, *27*, 570–574.
33. Gunawidjaja, R.; Peleshanko, S.; Ko, H.; Tsukruk, V. V. Bimetallic Nanocobs: Decorating Silver Nanowires with Gold Nanoparticles. *Adv. Mater.* **2008**, *20*, 1544.
34. Locatelli, E.; Ori, G.; Fournelle, M.; Lemor, R.; Montorsi, M.; Franchini, M. C. Click Chemistry for the Assembly of Gold Nanorods and Silver Nanoparticles. *Chem.—Eur. J.* **2011**, *17*, 9052–9056.
35. Israelachvili, J. N. *Intermolecular and Surface Forces*, 3rd ed.; Elsevier: San Diego, 2011.
36. Ashima, H.; Chun, W. J.; Asakura, K. Room-Temperature-Adsorption Behavior of Acetic Anhydride on a TiO_2(110) Surface. *Surf. Sci.* **2007**, *601*, 1822–1830.
37. Wang, P.; Wang, L. D.; Ma, B. B.; Li, B.; Qiu, Y. TiO_2 Surface Modification and Characterization with Nanosized PbS in Dye-Sensitized Solar Cells. *J. Phys. Chem. B* **2006**, *110*, 14406–14409.
38. Solbrand, A.; Henningsson, A.; Sodergren, S.; Lindstrom, H.; Hagfeldt, A.; Lindquist, S. E. Charge Transport Properties in Dye-Sensitized Nanostructured TiO_2 Thin Film Electrodes Studied by Photoinduced Current Transients. *J. Phys. Chem. B* **1999**, *103*, 1078–1083.
39. Santato, C.; Ulmann, M.; Augustynski, J. Photoelectrochemical Properties of Nanostructured Tungsten Trioxide Films. *J. Phys. Chem. B* **2001**, *105*, 936–940.
40. Decker, F.; Melsheimer, J.; Gerischer, H. Semiconductor-Oxide Heterojunctions as Electrodes in Photo-Electrochemical Cells. *Isr. J. Chem.* **1982**, *22*, 195–198.
41. Janotti, A.; Van de Walle, C. G. Absolute Deformation Potentials and Band Alignment of Wurtzite ZnO, MgO, and CdO. *Phys. Rev. B* **2007**, *75*, 121201.
42. Bessekhouad, Y.; Robert, D.; Weber, J. V. Photocatalytic Activity of Cu_2O/TiO_2, Bi_2O_3/TiO_2 and $ZnMn_2O_4/TiO_2$ Heterojunctions. *Catal. Today* **2005**, *101*, 315–321.
43. Liu, Z. Y.; Sun, D. D. L.; Guo, P.; Leckie, J. O. An Efficient Bicomponent TiO_2/SnO_2 Nanofiber Photocatalyst Fabricated by Electrospinning with a Side-by-Side Dual Spinneret Method. *Nano Lett.* **2007**, *7*, 1081–1085.
44. Sakthivel, S.; Geissen, S. U.; Bahnemann, D. W.; Murugesan, V.; Vogelpohl, A. Enhancement of Photocatalytic Activity by Semiconductor Heterojunctions: Alpha-Fe_2O_3, WO_3 and CdS Deposited on ZnO. *J. Photochem. Photobiol. A* **2002**, *148*, 283–293.
45. Izaki, M.; Shinagawa, T.; Mizuno, K. T.; Ida, Y.; Inaba, M.; Tasaka, A. Electrochemically Constructed P-Cu_2O/N-ZnO Heterojunction Diode for Photovoltaic Device. *J. Phys. D. Appl. Phys.* **2007**, *40*, 3326–3329.
46. Kumar, P. M.; Badrinarayanan, S.; Sastry, M. Nanocrystalline TiO_2 Studied by Optical, FTIR and X-Ray Photoelectron Spectroscopy: Correlation to Presence of Surface States. *Thin Solid Films* **2000**, *358*, 122–130.
47. Keller, V.; Bernhardt, P.; Garin, F. Photocatalytic Oxidation of Butyl Acetate in Vapor Phase on TiO_2, Pt/TiO_2 and WO_3/TiO_2 Catalysts. *J. Catal.* **2003**, *215*, 129–138.
48. Marmur, A. Ti-Surface Capillary Interactions. *Langmuir* **1993**, *9*, 1922–1926.
49. Wang, R.; Sakai, N.; Fujushima, A.; Watanabe, T.; Hashimoto, K. Studies of Surface Wettability Conversion on TiO_2 Single-Crystal Surfaces. *J. Phys. Chem. B* **1999**, *103*, 2188–2194.
50. Devaprakasam, D.; Biswas, S. K. Molecular Damping: Mechanical Response of Self-Assembled Monomolecular Layer to Compression. *Phys. Rev. B* **2005**, *72*, 125434.
51. Ito, S.; Murakami, T. N.; Comte, P.; Liska, P.; Gratzel, C.; Nazeeruddin, M. K.; Grätzel, M. Fabrication of Thin Film Dye Sensitized Solar Cells with Solar to Electric Power Conversion Efficiency over 10%. *Thin Solid Films* **2008**, *516*, 4613–4619.
52. Hara, K.; Horiguchi, T.; Kinoshita, T.; Sayama, K.; Sugihara, H.; Arakawa, H. Highly Efficient Photon-to-Electron Conversion with Mercurochrome-Sensitized Nanoporous Oxide Semiconductor Solar Cells. *Sol. Energy Mater. Sol. Cells* **2000**, *64*, 115–134.
53. Boulova, M.; Lucazeau, G. Crystallite Nanosize Effect on the Structural Transitions of WO_3 Studied by Raman Spectroscopy. *J. Solid State Chem.* **2002**, *167*, 42–434.
54. Kotsokechagia, T.; Cellesi, F.; Thomas, A.; Niederberger, M.; Tirelli, N. Preparation of Ligand-Free TiO_2 (Anatase) Nanoparticles through a Nonaqueous Process and Their Surface Functionalization. *Langmuir* **2008**, *24*, 6988–6997.
55. Shirley, D. A. High-Resolution X-Ray Photoemission Spectrum of the Valence Bands of Gold. *Phys Rev. B* **1972**, *5*, 4709–4714.
56. Tanuma, S.; Powell, C. J.; Penn, D. R. Calculations of Electron Inelastic Mean Free Paths for 31 Materials. *Surf. Interface Anal.* **1988**, *11*, 577–589.
57. Mora-Seró, I.; Dittrich, T.; Garcia-Belmonte, G.; Bisquert, J. Determination of Spatial Charge Separation of Diffusing Electrons by Transient Photovoltage Measurements. *J. Appl. Phys.* **2006**, *100*, 103705.
58. Anta, J. A.; Mora-Sero, I.; Dittrich, T.; Bisquert, J. Dynamics of Charge Separation and Trap-Limited Electron Transport in TiO_2 Nanostructures. *J. Phys. Chem. C* **2007**, *111*, 13997–14000.
59. Kronik, L.; Leibovitch, M.; Fefer, E.; Burstein, L.; Shapira, Y. Quantitative Surface Photovoltage Spectroscopy of Semiconductor Interfaces. *J. Electron. Mater.* **1995**, *24*, 379–385.